RSC Advances

RSC Publishing

PAPER

View Article Online
View Journal | View Issue

Cite this: *RSC Advances*, 2013, **3**, 12117

Molecular ordering and charge transport in a dicyanovinyl-substituted quaterthiophene thin film†

Chris Elschner,*[a] Manuel Schrader,[b] Roland Fitzner,[c] Alexandr A. Levin,‡[a] Peter Bäuerle,[c] Denis Andrienko,[b] Karl Leo[a] and Moritz Riede[a]

Received 2nd March 2013,
Accepted 16th May 2013

DOI: 10.1039/c3ra42184h

www.rsc.org/advances

By combining computer simulations, grazing incidence, and powder X-ray-diffraction measurements we reconstruct the crystal structure of a thin film of terminally dicyanovinyl-substituted quaterthiophene (DCV4T). The crystal structure differs from the known single crystal structure of the same compound, but resembles the molecular packing of a methylated DCV4T. Charge transport simulations on the molecular level show that the 2 dimensional thin-film charge-transport network is well suited for hole transport in solar cells.

I. Introduction

The efficiency of organic solar cells has seen an impressive increase in recent years,[1,2] reaching values of 12%.[3] Improvements stem from enhanced light absorption, better adjusted transport and excited state energy levels, and tuned (by appropriate substitutions and processing) donor–acceptor phase separation.[4–7]

In spite of these improvements, the field still lacks clear structure-property relations or, in other words, links between the chemical structure of the donor/acceptor and the device efficiency. To formulate such relationships, a better understanding of the molecular arrangement is required, especially in thin films and at donor–acceptor interfaces, since elementary processes such as exciton diffusion and splitting,[8–10] charge-carrier transport and extraction[11–19] are all very sensitive to electronic couplings and the shape of the electrostatic potential,[20–22] which intimately depends on positions and orientations of the molecules.

Neutron scattering,[23] solid-state nuclear magnetic resonance,[24–26] transmission electron microscopy (TEM)[27] and X-ray diffraction[28–33] are by now routinely used to gain insight into the local and global molecular packing. These experiments, however, are often performed on single crystals, in spite of the fact that the molecular ordering in a bulk crystal and in a thin film (used in a device) might not be identical. Macroscopic properties of organic materials, e. g. charge mobility, are known to sensitively depend on such ordering.[18,21] Thus, unveiling thin film molecular packing is imperative for understanding a connection between the device performance, molecular arrangement, and the underlying chemical structures.

In this work, we study molecular packing of dicyanovinyl end-capped quaterthiophene (DCV4T), a prototypical donor material for small-molecule solar cells,[6,7,34] the molecular structure of which is depicted in Fig. 1. We find that the new thin-film and the single crystal structures are different and that the thin-film structure resembles that of a single crystal of the methylated compound[6] (DCV4T–Me, Fig. 1). We then perform charge transport simulations on the molecular level with different molecular arrangements and demonstrate the impact of molecular packing on hole mobilities and solar cell efficiencies.

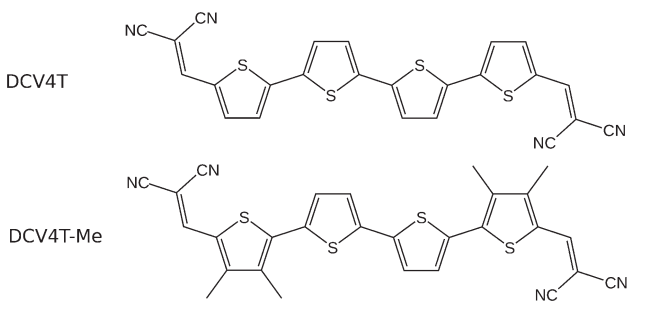

Fig. 1 Chemical structures of DCV4T and DCV4T–Me.

[a]*Institut für Angewandte Photophysik, TU-Dresden, George-Bähr-Str. 1, 01069 Dresden, Germany. E-mail: chris.elschner@iapp.de*
[b]*Max Planck Institute for Polymer Research, Ackermannweg 10, 55128 Mainz, Germany*
[c]*Institute of Organic Chemistry II and Advanced Materials, Albert-Einstein-Allee 11, 89081 Ulm, Germany*

† Electronic supplementary information (ESI) available: DCV4T thin film crystal structure. See DOI: 10.1039/c3ra42184h

‡ Current address: Max-Planck-Institut für Chemische Physik fester Stoffe, Nöthnitzer Str. 40, 01187 Dresden, Germany.

II. Methods

Experimental

DCV4T was purified by one vacuum sublimation and the same batch was used for all studies.[35] 50 nm thin films were prepared by thermally evaporating the powder in a vacuum chamber (pressure $<10^{-6}$ mbar) and depositing the material on a cleaned glass substrate at room temperature. The deposition rate of 0.2 Å s^{-1} was controlled by an oscillating quartz monitor.

Thin film XRD measurements have been carried out under asymmetric grazing incidence conditions (GIXRD) on a Bruker D8 Discover with 10 s sampling time per step.[29] Powder XRD measurements have been performed on an URD-6 powder diffractometer (Seifert FPM, Germany) in Bragg-Brentano geometry using Cu-Kα radiation and a scintillation detector. A 2θ-zero shift correction has been done with mica powder (NIST standard reference material 675). The sampling time was 60 s per step. An intensive mortaring of the powder in ethanol (between the measurements) and spinning (during the measurement) were used in order to reduce the influence of the (needle-like[34]) powder texture. The intensities of Bragg reflections did not change after the third mortaring and these measurements were used for the structural analysis.

Unit cell reconstruction

The algorithm used to reconstruct the unit cell from the powder diffraction data is described in ref. 29. Without going into details, it is based on matching the pair distribution functions (PDF). PDF is the real space pendant of the diffraction pattern, or a correlation function which quantifies deviations from the mean density on short scales (nanometers). As such, it is a measure of the distribution of atomic distances in the sample. The reference PDF is calculated from the measured powder diffraction pattern[29,36] by Fourier-transforming the nomalized scattering intensity. Using the reference PDF and the geometry of a single molecule (which is treated as a rigid body and was obtained from single crystal data[34]), the algorithm refines the unit cell and atomic coordinates until the best match of the PDF is achieved. Symmetry operations are not included in the algorithm, and therefore the reconstructed unit cell is given in the space group P1. The final unit cell is additionally refined using the Rietveld analysis.

Charge transport simulations

Charge transport simulations are performed using the different molecular arrangements of DCV4T. First, atomistic molecular dynamics simulations of a crystal super-cell of 2880 molecules have been carried out,[37] which introduces thermal disorder in the model. After this, charge hopping rates between neighboring molecules are evaluated using the high-temperature limit of the Marcus theory.[38,39] Finally the master equation for a diffusing charge carrier in a box with periodic boundary conditions was solved using the kinetic Monte Carlo algorithm.[40] All first principles calculations were performed with the GAUSSIAN[41] package, molecular dynamics simulations with the GROMACS[42] package, polarized site energy calculations using the Thole model[43] as implemented in TINKER,[44] and charge transport simulations with the VOTCA[40] package.

III. Results

The DCV4T thin film GIXRD pattern, shown in Fig. 2, has one strong Bragg reflection at $2\theta = 12.80^\circ$ ($d = 6.917$ Å) and several weaker ones (not shown) at $2\theta = 26.03^\circ$ and 29.03° ($d = 3.42$ Å and 3.08 Å, respectively) which indicates a high crystallinity and a preferred orientation of crystallites in the layer. The broadness of Bragg reflections is due to the small film thickness of about 50 nm and the resulting small crystallite sizes. Note that diffuse scattering from disordered or amorphous materials is not visible.[45]

The Bragg reflections of the powder XRD pattern, also shown in Fig. 2 and Fig. 4, are much sharper due to larger

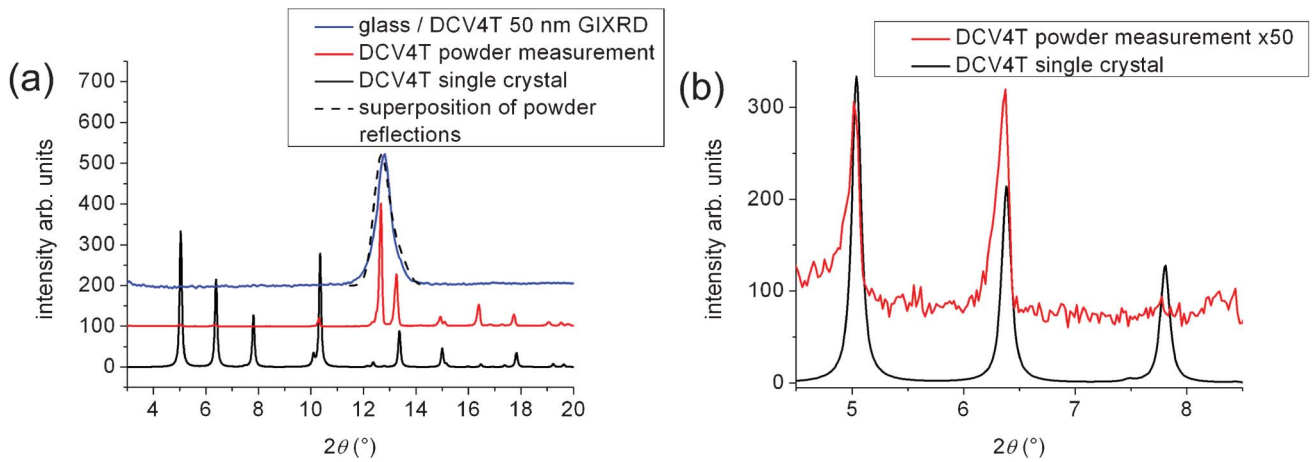

Fig. 2 XRD patterns of the DCV4T single crystal and powder, as well as the GIXRD thin film pattern in (a). (b) shows the powder and single crystal patterns with the powder pattern scaled by a factor of 50. Broadening and superposition of the two powder Bragg reections is depicted by a dashed line.

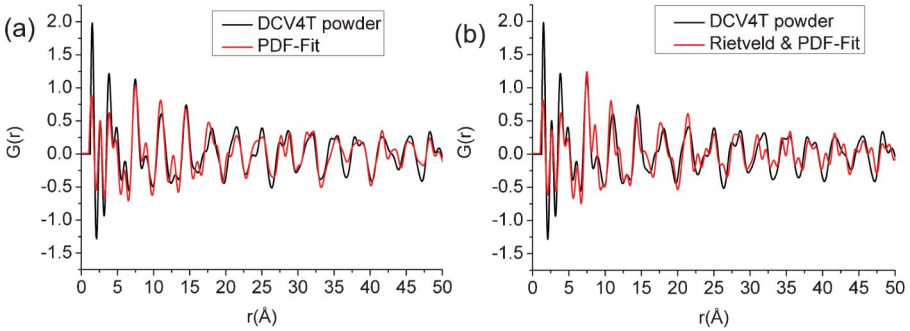

Fig. 3 PDFs of the DCV4T powder measurement in comparison to the PDF of the best fit structure model in (a), and the PDF of the Rietveld-refined structure model followed by a second PDF-fit in (b). The fitting is performed for $r < 30$ Å but a reasonable agreement is achieved also for larger distances.

crystallite sizes of around 85 nm, as estimated from the Scherrer equation. The position of one of the most intense reflections of the powder agree well with the position of the visible reflection of the thin film. A superposition of the two Gaussian-broadened powder reflections at $2\theta = 12.66^\circ$ and 13.25° matches the dominant reflection of the thin film (Fig. 2). The size of the thin film crystallites of 11.5 nm can be estimated from this broadening. Note that grazing incidence measurement conditions also result in peak broadening, hence this is only a rough (lower limit) estimate of crystallite sizes.

We should also mention that only one Bragg reflection of GIXRD measurements can be used for comparison with the powder data. 2D-GIWAXS (grazing incidence wide angle X-ray scattering) data are more suitable to obtain structure information from thin films due to the additional *in-plane* information.[28] The 2D-GIWAXS data of DCV4T:C60 layers[46] shows a Bragg reflection at $2\theta = 12.82^\circ$ in the *out-of-plane* direction, which is practically identical to the strong 1D GIXRD reflection. Another strong Bragg reflection at $2\theta = 26.03^\circ$ in the *in-plane* direction is not accessible to the 1D GIXRD measurements. Hence, both most intensive Bragg reflections of DCV4T can be found with low intensity in the powder (Fig. 4) as well as in the thin film samples (Fig. 2 and in ref. 46) at the same positions. We therefore conclude that the powder and the thin film have the same crystallographic phase and molecular packing.

At the same time, the DCV4T single crystal diffraction pattern obtained from simulations is different from the measured powder and thin film patterns (Fig. 2a). The first two Bragg reflections of the single crystal phase can still be found in the powder pattern (see Fig. 2b), and the strong reflection (or superposition of two reflections) of the thin film pattern does not match the single crystal data. Thus, the powder consists of at least two different crystallographic phases, with the single crystal phase being the minor phase. In order to reconstruct the crystal structure of the thin film, a pair distribution function (PDF) of the powder diffraction pattern is inverted as described in section II. The PDFs of the converged structure and the measured powder PDF are shown in Fig. 3b and the obtained unit cell parameters are listed in Table 1.[47] Note that there are several reason why the two PDFs do not perfectly agree. First, the PDF analysis optimizes the structure model according to a powder measurement which, however, is a mixture of two phases. Even though the amount of the minor phase (single crystal structure) is small, it still influences the

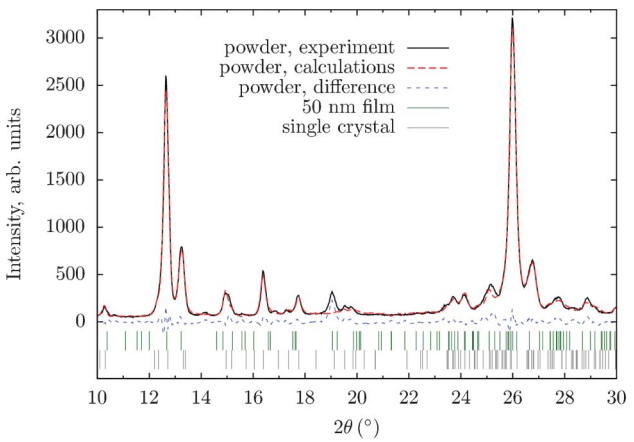

Fig. 4 XRD patterns of the DCV4T powder as measured, modeled using the PDF-fit procedure only, or combined PDF-fit and the Rietveld-refinement. The weight distribution is 98 wt.% and 2 wt.% for the DCV4T thin film and single crystal phases, respectively. The reference Bragg reflections of the DCV4T thin film and single crystal are also shown.

Table 1 Lattice parameters for the DCV4T thin film obtained using PDF-Fit before and after Rietveld fitting, as well as parameters for the DCV4T single crystal

	PDF-Fit	Rietveld	Single crystal[34]	DCV4T–Me
a (Å)	7.98(5)	7.64(9)	3.8295(8)	7.3763(9)
b (Å)	8.75(6)	8.61(7)	27.695(6)	8.8598(10)
c (Å)	18.66(14)	17.3(2)	22.663(5)	10.3120(12)
α (°)	90.6(3)	90.5(3)	90.00	103.718(3)
β (°)	67.7(6)	67.4(1.5)	91.68(3)	109.276(4)
γ (°)	99.8(4)	97.6(5)	90.00	91.233(4)
Z	2	2	4	1
V (Å^3)	1184.76	1038.87	2402.56	614.318
Symmetry	$P1$	$P1$	$P2_1/n$	$P-1$

quality of the fit. Second, XRD powder measurements are affected by the texture, even though we have tried to minimize its effect by mortaring. Finally, the algorithm is treating molecules as *rigid* bodies, *i.e.* neglects local disorder related to thermal fluctuations.

While the PDF provides direct information about the short range order of the molecular arrangement, the Bragg reflections in the diffraction pattern are linked to the periodicity of the crystalline structure and thereby provide information about the lattice parameters of the unit cell. Both ways of analyzing the data (in real or in reciprocal space) must lead to the same molecular arrangement. Here, the Rietveld technique[48] was used to further refine lattice parameters (hence, $a,b,c,\alpha,\beta,\gamma$ of the unit cell). The advantage of this technique is that it accounts for the influence of the texture and two phases in the film. The new thin film and the single crystal phases have been used together as initial phases for the Rietveld refinement. The refinement did not modify the atomic coordinates. Spherical harmonics were used to account for the influence of texture.

The results of the Rietveld analysis are shown in Fig. 4 and the modified lattice parameters are listed in Table 1. The analysis predicts the weight content of 98 wt.% for the DCV4T thin film and 2 wt.% for the single crystal phase in the powder. The model reached an agreement weighted profile factor of R_{wp} = 12.0%.[49] Finally, the Rietveld-refined thin film structure was again optimized using the PDF-fitting software. Now, the lattice parameters were constrained while positions and orientations of the DCV4T molecules in the (fixed) unit cell were allowed to change (Fig. 3 (b)). The molecular packing of this thin film structure is visualized in Fig. 5 (middle row). A pdb file of the new DCV4T thin film structure is available in the supplementary information†.

IV. Discussion and conclusions

Before discussing the implications of the different crystal structures on solar cell functionality, we compare the molecular arrangements of two similar compounds, DCV4T in the thin film structure and the structure of DCV4T–Me. Both are shown in Fig. 5 (middle and right), and are remarkably similar. The DCV4T–Me single crystal structure is likely to be identical to its thin film structure.[6] Hence, both compounds have similar packing in a thin film, *i.e.* in a solar cell device. The high similarity of the molecular packing of these both compounds, which have an almost identical molecular structure, can be seen as a proof of correctness of the DCV4T thin film structure.

The characteristic of an organic thin film solar cell depends on many different factors. One important issue is the charge carrier mobility towards the electrodes. Thus, it is important to have efficient charge carrier transport perpendicular to the electrodes. Since the GIXRD diffraction data provides the information about the molecular ordering perpendicular to the substrate, it is automatically linked to the crystal orientation relevant for the charge carrier transport in a solar cell.[50] In our case it is the 100 direction (*a*-axis of DCV4T thin film phase, see Fig. 5 (c)) or a superposition of the two Bragg reflections, 100 and 102. The pathway of the charge to the electrodes (within the crystalline regions of DCV4T) is the same for the neat layers than for blend layers with C60. That is why, the same Bragg reflection of DCV4T appears in neat layer DCV4T and in heated DCV4T:C60 blends in the *out of plane* direction.

In fact, the same situation is also observed in DCV4T–Me. Here, the 2θ-angle position of the Bragg reflection of a DCV4T–Me neat layer is identical to the position of DCV4T–Me Bragg reflection in a blend with C_{60} (evaporated on a heated substrate).[6] This thin film reflection can be identified with the single crystal reflection 010 (*b*-axis of DCV4T–Me phase, see Fig. 5 (c)) or a superposition of 010 and $01\bar{1}$. Calculated charge carrier mobilities for these crystal directions are listed in Table 2, indicating that DCV4T–Me has a slightly higher hole mobility than DCV4T in the direction perpendicular to the electrodes. Comparing the molecular orientation of DCV4T (along *a*-axis) and DCV4T–Me (along *b*-axis) shows a similar molecular stacking of both molecule types on the surface of the substrate, in Fig. 5 (c).

Another important observation can be made by comparing charge transport in the single crystal phase and the thin film phase of DCV4T. The crystal structure of the DCV4T single crystal has a distinct direction with strong electronic couplings.[37] Counterintuitively, this topology of the charge transporting network is not beneficial: strong electronic couplings in one direction tend to suppress couplings in the other directions and, when combined with the substantial energetic disorder, are prone to charge trapping and hence low mobilities. Contrary, the topology of the charge transporting network in DCV4T–Me is more diverse and less affected by the energetic disorder. Since our results indicate that the crystal structure of the DCV4T thin film is similar to the single crystal structure of DCV4T–Me, one might expect that the charge carrier mobility of DCV4T is higher in the thin film structure than in the single crystal structure.

To confirm this, the transporting networks of DCV4T in a single crystal and a thin film phase, as well as DCV4T–Me crystal are shown in Fig. 5. One can see that the DCV4T–Me and DCV4T thin film networks are similar, with less pronounced one-dimensional character as compared to the DCV4T single crystal structure. This has an immediate implication on charge mobility: the simulated mobility of the DCV4T thin film phase (maximum value of 2.9×10^{-2} cm^2 V^{-1} s^{-1}) is more than an order of magnitude higher than that of the DCV4T single crystal (maximum value of 1.1×10^{-3} cm^2 V^{-1} s^{-1}). Note, that the energetic disorder is the same for both systems and the higher mobility is due to an advantageous topology of the charge transporting network (electronic coupling elements).

A detailed analysis of the small differences between the DCV4T thin film structure and the DCV4T–Me structure reveals a higher symmetry in case of the DCV4T–Me. The

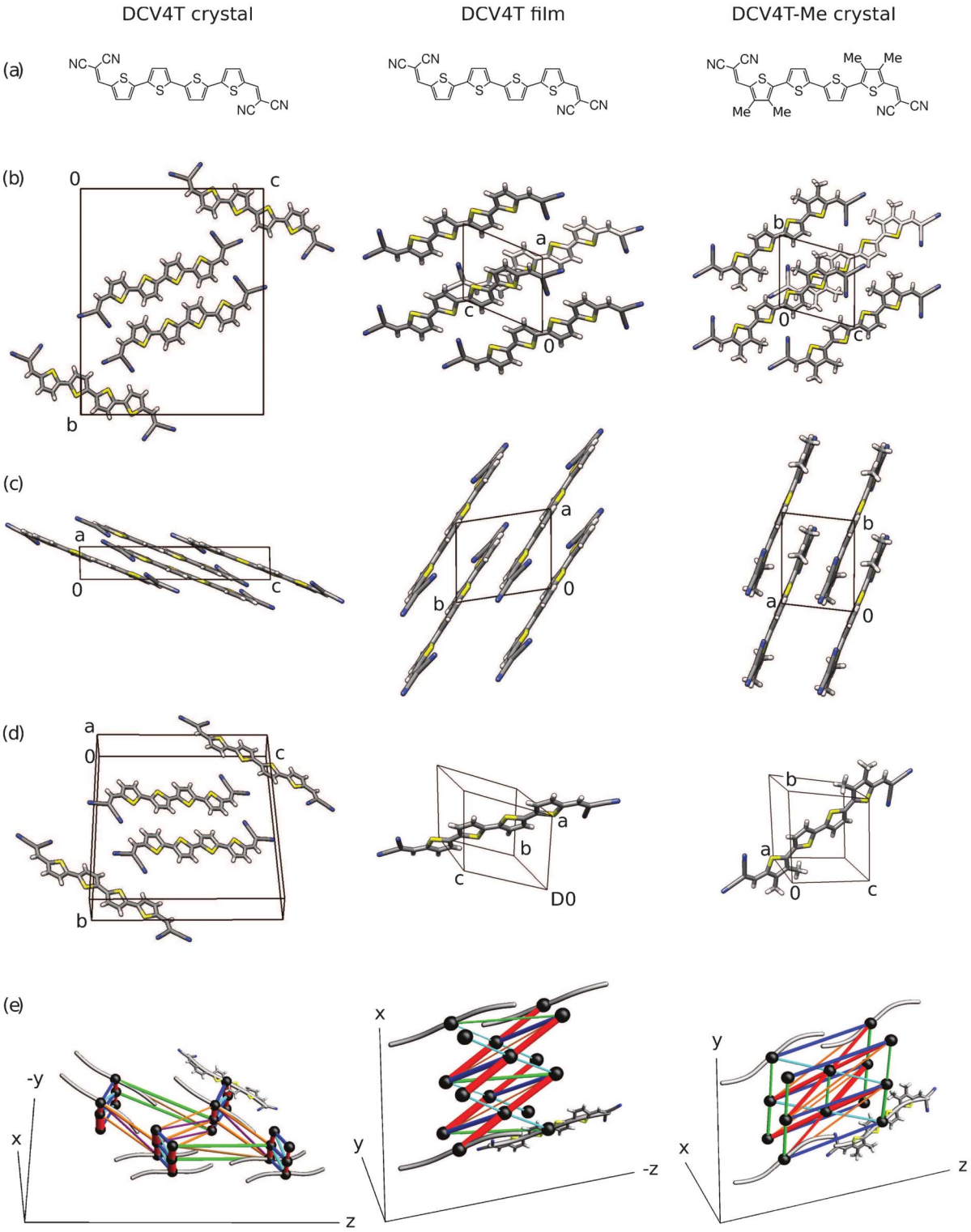

Fig. 5 (a–d) Unit cells of DCV4T (single crystal), DCV4T (thin film) and DCV4T–Me (crystal). Orientations are chosen to emphasize similarity between the two structures DCV4T (film) and DCV4T–Me (crystal). Note that the DCV4T (film) unit cell has been reduced to one molecule (The DCV4T thin film crystal structure contains two molecules per unit cell with only very small deviations concerning the orientation of these. Therefore the reduction to one molecule per unit cell is in good approximation possible.) (e) Charge transport networks of DCV4T and DCV4T–Me single crystals as well as DCV4T thin film. Here, the centers of mass of the molecules are shown as black spheres, while electronic couplings are shown as edges whose thickness is proportional to the logarithm of the average coupling elements. Colors reflect distinct transport directions in a unit cell.

Table 2 Simulated charge carrier mobilities for the indicated lattice directions of the DCV4T thin film and DCV4T–Me single crystal structures. These crystal orientations are relevant for charge transport in organic solar cells

	DCV4T thin film	DCV4T thin film	DCV4T–Me	DCV4T–Me
hkl	100	102	010	$01\bar{1}$
2θ (°)	12.66	13.25	10.34	12.05
μ ($cm^2\ V^{-1}\ s^{-1}$)	1.6×10^{-2}	3.6×10^{-3}	8.7×10^{-2}	1.5×10^{-2}

DCV4T–Me molecules in the upper row cover the two molecules below each by half (see Fig. 5 (b) for DCV4T thin film and DCV4T–Me). On the other hand, in the DCV4T thin film structure, the upper molecule is only shifted by 33% (not by 48% as in the case of DCV4T–Me, 50% would be completely symmetrical). Thus, the DCV4T molecules don't have such a symmetrical covering like the DCV4T–Me. This symmetrical covering, in case of DCV4T–Me, tends to be optimal for charge carrier transport and results in the highest charge carrier mobility (maximum value of 1.6×10^{-1} $cm^2\ V^{-1}\ s^{-1}$). The increase of symmetry results in an increase of charge carrier mobility, by adding new, easy accessable pathways for charge carrier transport. Hence, a further improvement of the charge carrier transport properties based on this structure (DCV4T thin film and DCV4T–Me) should not be expected by a slightly rearrangement of the molecular packing. The almost optimal arrangement with the highest symmetry is still achieved for DCV4T–Me.

A direct comparison of simulation results to experimental data is, however, not possible, due to lack of (orientation-dependent) single crystal mobility measurements. OFET mobilities of these compounds are available and are of the order of 10^{-4} $cm^2\ V^{-1}\ s^{-1}$.[6] The absolute values are of course much lower than those calculated here since OFET has polycrystalline order. Nevertheless, DCV4T–Me has higher mobility than DCV4T,[6] which is in agreement with simulation results. Moreover, the DCV4T-based solar cell has efficiency of 1.5%, while the efficiency of the DCV4T–Me cell is 3.8%, which correlates with the better hole mobility in DCV4T–Me.

To summarize, lattice parameters and molecular packing of a thin vacuum-deposited film of DCV4T is determined by inverting its X-ray powder diffraction pattern. We find that crystal structures of the powder (major component) and the thin film are identical but differ from the previously reported single crystal structure of DCV4T. The identified thin film packing is shown to be similar to the single crystal structure of DCV4T–Me and is found to be beneficial for hole transport in crystal directions relevant to thin-film small-molecule based organic solar cells.

Acknowledgements

This work was partially supported by the DFG program IRTG 1404, DFG grant SPP 1355, BMBF projects MESOMERIE (13N11704) and OPA (13N9872). We are grateful to Mara Jochum, Kostas Daoulas, and Carl Pölking for critical reading of the manuscript, as well as Christian Koerner and Heliatek GmbH for fruitful discussions and technical support.

References

1 M. A. Green, K. Emery, Y. Hishikawa, W. Warta and E. D. Dunlop, *Prog. Photovoltaics*, 2011, **20**, 12.
2 http://www.orgworld.de/, accessed 01/02/2012.
3 Press release Heliatek GmbH, accessed 19/01/2013.
4 V. Steinmann, N. M. Kronenberg, M. R. Lenze, S. M. Graf, D. Hertel, H. Bürckstümmer, F. Würthner and K. Meerholz, *Appl. Phys. Lett.*, 2011, **99**, 193306.
5 V. Steinmann, N. M. Kronenberg, M. R. Lenze, S. M. Graf, D. Hertel, K. Meerholz, H. Bürckstümmer, E. V. Tulyakova and F. Würthner, *Adv. Energy Mater.*, 2011, **1**, 888–893.
6 R. Fitzner, C. Elschner, M. Weil, C. Uhrich, C. Körner, M. Riede, K. Leo, M. Pfeiffer, E. Reinold and E. Mena-Osteritz, *et al.*, *Adv. Mater.*, 2012, **24**, 675–680.
7 A. Mishra and P. Bäuerle, *Angew. Chem., Int. Ed.*, 2012, **51**, 2020–2067.
8 T. A. Papadopoulos, L. Muccioli, S. Athanasopoulos, A. B. Walker, C. Zannoni and D. Beljonne, *Chem. Sci.*, 2011, **2**, 1025.
9 B. Baumeier, D. Andrienko, Y. Ma and M. Rohlfing, *J. Chem. Theory Comput.*, 2012, **8**, 997.
10 B. Baumeier, D. Andrienko and M. Rohlfing, *J. Chem. Theory Comput.*, 2012, **8**, 2790.
11 J. Kirkpatrick, V. Marcon, J. Nelson, K. Kremer and D. Andrienko, *Phys. Rev. Lett.*, 2007, **98**, 227402.
12 F. Ortmann, F. Bechstedt and K. Hannewald, *Physica Status Solidi (b)*, 2011, **248**.
13 T. Vehoff, B. Baumeier, A. Troisi and D. Andrienko, *J. Am. Chem. Soc.*, 2010, **132**, 11702.
14 D. L. Cheung and A. Troisi, *Phys. Chem. Chem. Phys.*, 2008, **10**, 5941.
15 J.-L. Brédas, J. E. Norton, J. Cornil and V. Coropceanu, *Acc. Chem. Res.*, 2009, **42**, 1691.
16 V. Marcon, D. W. Breiby, W. Pisula, J. Dahl, J. Kirkpatrick, S. Patwardhan, F. Grozema and D. Andrienko, *J. Am. Chem. Soc.*, 2009, **131**, 11426.
17 J. Nelson, J. J. Kwiatkowski, J. Kirkpatrick and J. M. Frost, *Acc. Chem. Res.*, 2009, **42**, 1768.
18 M. Schrader, C. Körner, C. Elschner and D. Andrienko, *J. Mater. Chem.*, 2012.
19 B. Baumeier, F. May, C. Lennartz and D. Andrienko, *J. Mater. Chem.*, 2012, **22**, 10971.

20 J. Idé, S. Mothy, A. Savoyant, A. Fritsch, P. Aurel, R. Méreau, L. Ducasse, J. Cornil, D. Beljonne and F. Castet, *Int. J. Quantum Chem.*, 2013, **113**, 580–584.
21 S. Mothy, M. Guillaume, J. Idé, F. Castet, L. Ducasse, J. Cornil and D. Beljonne, *J. Phys. Chem. Lett.*, 2012, **3**, 2374.
22 S. Verlaak, D. Beljonne, D. Cheyns, C. Rolin, M. Linares, F. Castet, J. Cornil and P. Heremans, *Adv. Funct. Mater.*, 2009, **19**, 3809–3814.
23 G. M. Newbloom, F. S. Kim, S. A. Jenekhe and D. C. Pozzo, *Macromolecules*, 2011, **44**, 3801.
24 T. Fukushima, H. Kimura, Y. Shimahara and H. Kaji, *Appl. Phys. Lett.*, 2011, **99**, 223301.
25 F. May, V. Marcon, M. R. Hansen, F. Grozema and D. Andrienko, *J. Mater. Chem.*, 2011, **21**, 9538.
26 N. C. Miller, E. Cho, M. J. N. Junk, R. Gysel, C. Risko, D. Kim, S. Sweetnam, C. E. Miller, L. J. Richter and R. J. Kline, *et al.*, *Adv. Mater.*, 2012, 6071–6079.
27 S. Pfuetzner, C. Mickel, J. Jankowski, M. Hein, J. Meiss, C. Schuenemann, C. Elschner, A. A. Levin, B. Rellinghaus and K. Leo, *et al.*, *Org. Electron.*, 2011, **12**, 435.
28 H. Sirringhaus, P. J. Brown, R. H. Friend, M. M. Nielsen, K. Bechgaard, B. M. W. Langeveld-Voss, A. J. H. Spiering, R. a. J. Janssen, E. W. Meijer and P. Herwig, *et al.*, *Nature*, 1999, **401**, 685.
29 C. Elschner, A. A. Levin, L. Wilde, J. Grenzer, C. Schroer, K. Leo and M. Riede, *J. Appl. Crystallogr.*, 2011, **44**, 983.
30 V. Marcon, J. Kirkpatrick, W. Pisula and D. Andrienko, *Phys. Status Solidi B*, 2008, **245**, 820–824.
31 H. N. Tsao, D. Cho, J. W. Andreasen, A. Rouhanipour, D. W. Breiby, W. Pisula and K. Müllen, *Adv. Mater.*, 2009, **21**, 209.
32 E. Cho, C. Risko, D. Kim, R. Gysel, N. Cates Miller, D. W. Breiby, M. D. McGehee, M. F. Toney, R. J. Kline and J.-L. Bredas, *J. Am. Chem. Soc.*, 2012, **134**, 6177.
33 X. Lu, H. Hlaing, D. S. Germack, J. Peet, W. H. Jo, D. Andrienko, K. Kremer and B. M. Ocko, *Nat. Commun.*, 2012, **3**, 795.
34 R. Fitzner, E. Reinold, A. Mishra, E. Mena-Osteritz, H. Ziehlke, C. Körner, K. Leo, M. Riede, M. Weil and O. Tsaryova, *et al.*, *Adv. Funct. Mater.*, 2011, **21**, 897.
35 The same batch was used for X-ray studies of single crystals, grown by subliming the DCV4T powder. Single crystal crystal structure is available in ref. 34.
36 T. Proffen, S. J. L. Billinge, T. Egami and D. Louca, *Z. Kristallogr.*, 2003, **218**, 132.
37 M. Schrader, R. Fitzner, M. Hein, C. Elschner, B. Baumeier, K. Leo, M. Riede, P. Bäuerle and D. Andrienko, *J. Am. Chem. Soc.*, 2012, **134**, 6052.
38 R. A. Marcus, *Rev. Mod. Phys.*, 1993, **65**, 599.
39 G. R. Hutchison, M. A. Ratner and T. J. Marks, *J. Am. Chem. Soc.*, 2005, **127**, 2339.
40 V. Rühle, A. Lukyanov, F. May, M. Schrader, T. Vehoff, J. Kirkpatrick, B. Baumeier and D. Andrienko, *J. Chem. Theory Comput.*, 2011, **7**, 3335.
41 M. J. Frisch, J. Jaramillo, R. Gomperts, R. E. Stratmann, O. Yazyev, A. J. Austin, R. Cammi, C. Pomelli, J. W. Ochterski and P. Y. Ayala, *et al.*, *Gaussian 03, Revision C.02 (2004)*, Gaussian, Inc., Wallingford, CT, 2004.
42 B. Hess, C. Kutzner, D. van der Spoel and E. Lindahl, *J. Chem. Theory Comput.*, 2008, **4**, 435.
43 B. Thole, *Chem. Phys.*, 1981, **59**, 341.
44 J. W. Ponder, C. Wu, P. Ren, V. S. Pande, J. D. Chodera, M. J. Schnieders, I. Haque, D. L. Mobley, D. S. Lambrecht and R. A. DiStasio, *et al.*, *J. Phys. Chem. B*, 2010, **114**, 2549.
45 Diffusive scattering can be seen in co-evaporated DCV4T and C_{60} blend layers (ref. 46).
46 C. Koerner, C. Elschner, N. C. Miller, R. Fitzner, F. Selzer, E. Reinold, P. Bäuerle, M. F. Toney, M. D. McGehee and K. Leo, *et al.*, *Org. Electron.*, 2012, **13**, 623.
47 The mismatch for interatomic correlation distances below 5 Å is due to low energies of Cu-radiation used in X-ray measurements. Since Cu-radiation gives only a maximum magnitude of the scattering vector up to Q = 8 $Å^{-1}$ this leads to termination ripples in the low r-region of the PDF after the Fourier transformation (ref. 29,51).
48 Bruker, *TOPAS. Version 2.0*, Bruker AXS, Karl-sruhe, Germany, 2000.
49 A Bragg reflection at $2\theta = 19.04^\circ$ is not reproduced by this model, even though reflections close to this position exist both in the DCV4T thin film phase ($1\bar{1}3$ at $2\theta = 19.054^\circ$) and in the single crystal phase[34] (0 6 0 at $2\theta = 19.222^\circ$).
50 Due to the asymmetric measurement conditions it is tilted by $\approx 6^\circ$.
51 P. F. Peterson, E. S. Božin, T. Proffen and S. J. L. Billinge, *J. Appl. Crystallogr.*, 2003, **36**, 53.